

On the Entanglement of Multiple CFTs via Rotating Black Hole Interior

Norihiro Iizuka^{1,*} and Noriaki Ogawa^{2,†}

¹*Interdisciplinary Fundamental Physics Team, Interdisciplinary
Theoretical Science Research Group, RIKEN, Wako 351-0198, JAPAN*
²*School of Physics, Korea Institute for Advanced Study, Seoul 130-722, Korea*

We study the minimal surfaces between two of the multiple boundaries of 3d maximally extended rotating eternal black hole. Via AdS/CFT, this corresponds to investigating the behavior of entanglements of the boundary CFT with multiple sectors. Non-trivial time evolutions of such entanglements detect the geometry inside the horizon, and behave differently depending on the choice of the two boundaries.

I. INTRODUCTION

The gauge/gravity correspondence is a fascinating correspondence. In short, it gives the non-perturbative definition of quantum gravity in terms of the corresponding gauge theories. However, how and why the bulk spacetime and gravity appears out of the boundary theory is still in obscurity, and indeed it is one of the most fundamental questions in this correspondence.

Van Raamsdonk [1, 2] pointed out that quantum entanglement between separated regions of the boundary theory is a key to the emergence of smoothly connectedness of the spacetime in the bulk. This idea has been extended and materialized in subsequent works, for example [3, 4]. Especially in Hartman-Maldacena [3], they investigated the time evolution of entanglement between the two copies of boundary CFT, in eternal AdS black hole without angular momentum. In this letter, we extend the analysis of [3] to the case of rotating BTZ black hole. Unlike the non-rotating case, the spacetime boundary has 8 disconnected regions. Naively they seem to correspond to 8 decoupled sectors of the boundary CFT, which are (maximally) entangled to one another. However, as we will see, actually the story is not so simple.

This short letter is organized as follows. We first review the known global structure of the rotating BTZ black hole very briefly in section II (a bit more details are given in Appendices A,B). Then, we derive the lengths of the geodesics connecting the different boundaries in section III, and by using it, calculate the entanglement between different boundaries in section IV using the holographic entanglement formula [5, 6]. We will discuss and interpret the results in section V.

II. ROTATING BTZ AND ANALYTIC CONTINUATION

The rotating BTZ black hole geometry is expressed as

$$ds^2 = -f(r)dt^2 + \frac{dr^2}{f(r)} + r^2(d\phi - N(r)dt)^2, \quad (1)$$

$$f(r) = \frac{(r^2 - r_+^2)(r^2 - r_-^2)}{r^2}, \quad N(r) = \frac{r_+ r_-}{r^2}, \quad (2)$$

where $\phi \simeq \phi + 2\pi$. We set AdS scale to be unit in this letter. The outer/inner horizon radii r_+ and r_- are related to the ‘‘chiral temperatures’’ T_+ and T_- ($T_+ \leq T_-$) as $r_{\pm} = \pi(T_- \pm T_+)$.

This geometry is obtained by an orbifold on the global AdS₃, and the outer region of the horizon ($r > r_+$) can be embedded in $\mathbb{R}^{2,2}$, where $ds^2 = -dx_0^2 - dx_1^2 + dx_2^2 + dx_3^2$, as

$$x_1 = \eta_1 \left(\frac{r^2 - r_-^2}{r_+^2 - r_-^2} \right)^{1/2} \cosh(\pi(T_+ u^+ + T_- u^-)), \quad (3a)$$

$$x_2 = \eta_1 \left(\frac{r^2 - r_-^2}{r_+^2 - r_-^2} \right)^{1/2} \sinh(\pi(T_+ u^+ + T_- u^-)), \quad (3b)$$

$$x_3 = \eta_2 \left(\frac{r^2 - r_+^2}{r_+^2 - r_-^2} \right)^{1/2} \cosh(\pi(T_+ u^+ - T_- u^-)), \quad (3c)$$

$$x_0 = \eta_2 \left(\frac{r^2 - r_+^2}{r_+^2 - r_-^2} \right)^{1/2} \sinh(\pi(T_+ u^+ - T_- u^-)), \quad (3d)$$

where $u^{\pm} = \phi \pm t$ and $\eta_i = \pm 1$. The four combinations of the (η_1, η_2) represents distinct regions outside the black hole, which we call 1_{++} , 1_{+-} , 1_{-+} and 1_{--} . One can go from one to another only through the interior region. We explain the spacetime structure of this geometry slightly more in Appendix A. The orbifold to produce the periodicity for ϕ is given in (A5). For more details, see [7].

Furthermore, these different regions can be connected to one another by analytic continuations of (t, ϕ) or u^{\pm} coordinates to complex-valued regions, as TABLE I.

III. GEODESICS BETWEEN BOUNDARIES

Our purpose in this paper is to investigate the way how the degrees of freedom on different boundaries are

*Electronic address: norihiro.iizuka@riken.jp;
Address after April 1, 2014: *Department of Physics,
Osaka University, Toyonaka, Osaka 560-0043, JAPAN*
†Electronic address: noriaki@kias.re.kr

| | u^+ | u^- | r |
|----------|------------------------|------------------------|-----|
| 1_{++} | u^+ | u^- | r |
| 1_{--} | $u^+ - \frac{i}{T_+}$ | u^- | r |
| 1_{+-} | $u^+ - \frac{i}{2T_+}$ | $u^- + \frac{i}{2T_-}$ | r |
| 1_{-+} | $u^+ - \frac{i}{2T_+}$ | $u^- - \frac{i}{2T_-}$ | r |

TABLE I: Analytic continuations from 1_{++} to $1_{\eta_1\eta_2}$, up to the periodicity $(u^+, u^-) \simeq (u^+ + i/T_+, u^- \pm i/T_-)$. Their complex conjugates also work.

| | X_n |
|----------|--|
| 1_{++} | $\sinh(\pi T_- (\delta u^- + 2\pi n)) \sinh(\pi T_+ (\delta u^+ + 2\pi n))$ |
| 1_{--} | $-\sinh(\pi T_- (\delta u^- + 2\pi n)) \sinh(\pi T_+ (\delta u^+ + 2\pi n))$ |
| 1_{+-} | $\cosh(\pi T_- (\delta u^- + 2\pi n)) \cosh(\pi T_+ (\delta u^+ + 2\pi n))$ |
| 1_{-+} | $-\cosh(\pi T_- (\delta u^- + 2\pi n)) \cosh(\pi T_+ (\delta u^+ + 2\pi n))$ |

TABLE II: Lengths $L^{(n)}(P_1, P_2)$ of geodesics connecting P_1 on 1_{++} boundary and P_2 on each boundary, in terms of X_n where $L^{(n)}(P_1, P_2) = \log X_n - \log(\pi^2 T_+ T_-) + \log r_\infty^2$ and $\delta u^\pm = u_2^\pm - u_1^\pm$.

entangled. In 2d CFT, various entanglement entropies are expressed as combinations of the lengths of geodesics connecting points on the boundaries of the 3d spacetime, according to the Ryu-Takayanagi holographic entanglement entropy formula [5, 6].

First, we consider two points $P_1 = (t_1, \phi_1, r_\infty)$ and $P_2 = (t_2, \phi_2, r_\infty)$ on the boundary of the same region, say 1_{++} . The geodesic length connecting P_1 and P_2 is easily computed by the coordinate mapping to Poincare AdS₃ [8], giving

$$\begin{aligned}
L_{1_{++}}^{(n)}(P_1, P_2) &= \log X_n - \log(\pi^2 T_+ T_-) + \log r_\infty^2, \\
X_n &= \sinh(\pi T_- (\delta u^- + 2n\pi)) \sinh(\pi T_+ (\delta u^+ + 2n\pi)), \\
\delta u^\pm &= u_2^\pm - u_1^\pm,
\end{aligned} \tag{4}$$

where $n \in \mathbb{Z}$ is the “winding number” around the ϕ -circle (2). The minimum $X = \min_{n \in \mathbb{Z}} \{X_n\}$ is positive, if and only if P_1 and P_2 are spacelike separated on the cylindrical boundary of 1_{++} .

By applying the analytic continuation TABLE I for the point P_2 in (4), we obtain the geodesic length between 1_{++} and another boundary, as TABLE II.

From this TABLE II, we notice that X_n are always positive for 1_{+-} and negative for 1_{-+} . It implies that whole of the 1_{+-} boundary is spacelike separated to 1_{++} boundary, while the 1_{-+} boundary is timelike. The most complicated is the case of 1_{--} . By taking very large winding number n , we can make X_n arbitrarily negative, that is, make the geodesic more timelike.

IV. ENTANGLEMENT BETWEEN DIFFERENT BOUNDARIES

When we take a proper time-slice in this spacetime which connects the boundaries of 1_{++} and 1_{+-} , the

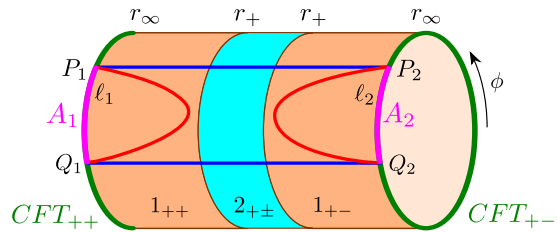


FIG. 1: The subsystem $A = A_1 \cup A_2$ and the corresponding candidates of the minimal surface, when A_2 is on the boundary of 1_{+-} . Red lines: the “disconnected” surface (eq.(6)). Blue lines: one of the “connected” surfaces across the horizon (eq.(7), $n = 0$). Although the time direction is not drawn here, those lines do not live on the same time slice in general.

boundary dual is discussed in [9] — it is a maximally entangled pair of two CFT sectors with chiral temperatures $T_+ \neq T_-$ (in other words, with chemical potential for momentum). We expect that it would also be true when we take different time-slices connecting other boundary pairs.

In order to investigate the structures of such inter-boundary entanglement, we consider the entanglement entropy for a subsystem A which is the union of two intervals A_1 and A_2 on different boundaries (FIG. 1). We fix A_1 on the boundary of 1_{++} , and A_2 is on another one (in FIG. 1, 1_{+-}).

We set the endpoints of A_1 and A_2 as $P_1 = (t_1, \phi_1, r_\infty)$, $Q_1 = (t_1, \phi_1 + \ell_1, r_\infty)$ and $P_2 = (t_2, \phi_2, r_\infty)$, $Q_2 = (t_2, \phi_2 + \ell_2, r_\infty)$, respectively, where $0 < \ell_1, \ell_2 < 2\pi$.

According to the minimal area prescription [5, 6], the corresponding entanglement entropy is given by

$$S_A = \min \left\{ S_A^{(c)}, S_A^{(d)} \right\}, \tag{5}$$

$$S_A^{(d)} = L^{(0)}(P_1, Q_1) + L^{(0)}(P_2, Q_2), \tag{6}$$

$$S_A^{(c)} = \min \left\{ L^{(n)}(P_1, P_2) + L^{(n)}(Q_1, Q_2) \mid n \in \mathbb{Z} \right\}, \tag{7}$$

¹ where we set $4G_N = 1$ for simplicity. These $S_A^{(d)}$ and $S_A^{(c)}$ correspond to different topologies of the minimal surface drawn in FIG.1 by red (“disconnected”) and blue (“connected”) lines². Physical quantity

$$I(A_1, A_2) = S_{A_1} + S_{A_2} - S_A, \tag{8}$$

plays the role of the order parameter which distinguishes these two phases. That is, the red disconnected surface

¹ Actually $S_A^{(d)}$ has another candidate which corresponds to the surface going around the other side of the ϕ -circle (with winding number $n = -1$). Hereafter we assume that (6) (red line in FIG.1) is always smaller than it. This is possible without loss of generality because we can redefine $A_i \rightarrow A_i^c$ and $\ell_i \rightarrow 2\pi - \ell_i$ ($i = 1, 2$ at the same time) without changing $S_A^{(c)}$ (7).

² In the connected phase, the two geodesics in (7) must have same winding numbers, in order that the union of the two geodesics should be homotopic to A .

corresponds to $I(A_1, A_2) = 0$ phase while the blue connected one is $I(A_1, A_2) > 0$ phase, and it is a sharp phase transition only in the classical approximation, i.e., large N on the CFT side [3, 10]³.

The entanglement entropy of the disconnected phase $S_A^{(d)}$ (6) can be written as

$$S_A^{(d)} = \log[\sinh(\pi T_- \ell_1) \sinh(\pi T_+ \ell_1) \sinh(\pi T_- \ell_2) \sinh(\pi T_+ \ell_2)] - 2 \log(\pi^2 T_+ T_-) + 2 \log r_\infty^2, \quad (9)$$

regardless of which boundary A_2 lives on. In particular, when the black hole is nearly extremal, we have $T_+^{-1} \gg \ell_i$ and then

$$S_A^{(d)} \simeq \log[\sinh(\pi T_- \ell_1) \sinh(\pi T_- \ell_2)] + \log(\ell_1 \ell_2) - 2 \log(\pi T_-) + 2 \log r_\infty^2. \quad (10)$$

A. $(1_{++}, 1_{+-})$

First let us put A_2 in Region 1_{+-} . This is what corresponds to the setup investigated in [3]. Let us take

$$\phi_2 - \phi_1 = \delta\phi, \quad \ell_2 - \ell_1 = \delta\ell, \quad t_2 - t_1 = \delta t, \quad (11)$$

Since the time coordinate t flows to opposite directions between 1_{++} and 1_{+-} regions, we regard this δt as the time flow of the total system. From TABLE II, we obtain

$$\begin{aligned} S_A^{(c)} &= \log X_n^P + \log X_n^Q - 2 \log(\pi^2 T_+ T_-) + 2 \log r_\infty^2, \\ X_n^P &= \cosh(\pi T_- (\delta\phi - \delta t + 2\pi n)) \\ &\quad \times \cosh(\pi T_+ (\delta\phi + \delta t + 2\pi n)), \\ X_n^Q &= \cosh(\pi T_- (\delta\phi - \delta t + \delta\ell + 2\pi n)) \\ &\quad \times \cosh(\pi T_+ (\delta\phi + \delta t + \delta\ell + 2\pi n)). \end{aligned} \quad (12)$$

Of course, when $T_- = T_+$, $\delta\phi = \delta\ell = 0$ and $n = 0$, this reproduces the corresponding result in [3] (eq.(3.32)).

Furthermore, one can show that

$$S_A^{(c)} > 4\pi T_+ |\delta t| - 4 \log 2 - 2 \log(\pi^2 T_+ T_-) + 2 \log r_\infty^2, \quad (13)$$

for arbitrary choice of n . Therefore in any cases, $S_A^{(c)}$ becomes very large in proportion to $|\delta t|$, therefore $S_A^{(d)} < S_A^{(c)}$ and $S_A = S_A^{(d)}$ in late time.

In particular, in near-extremal case, we find that the right-hand side also has a very large constant term $-2 \log T_+$. It corresponds to the divergence of the distance to the horizon in the extremal black hole, which can also be observed in the case of 5D non-rotating charged extremal black hole [11]. In terms of the boundary theory, it is closely related to the residual entropy, coming from IR degrees of freedom. As a result, the disconnected phase is always favored and we experience no transition in the near-extremal setup.

B. $(1_{++}, 1_{--})$

When we put A_2 in Region 1_{+-} in the same way as (11), we obtain from TABLE II

$$\begin{aligned} S_A^{(c)} &= \log X_n^P + \log X_n^Q - 2 \log(\pi^2 T_+ T_-) + 2 \log r_\infty^2, \\ X_n^P &= -\sinh(\pi T_- (\delta\phi - \delta t + 2\pi n)) \\ &\quad \times \sinh(\pi T_+ (\delta\phi + \delta t + 2\pi n)), \\ X_n^Q &= -\sinh(\pi T_- (\delta\phi - \delta t + \delta\ell + 2\pi n)) \\ &\quad \times \sinh(\pi T_+ (\delta\phi + \delta t + \delta\ell + 2\pi n)). \end{aligned} \quad (14)$$

As we noted at the end of the previous section, these X_n^P and X_n^Q are not positive in general. They tend to be positive in late time for fixed values of n , but for any fixed time and other parameters, they become negative by taking sufficiently large n .

To avoid this strange property of the periodicity, let us consider a decompactifying limit and ignore the windings (i.e., set $n = 0$)⁴. After fixing $n = 0$, the lengths of the both geodesics are real when $\delta t > \delta t_0 \equiv \max\{|\delta\phi|, |\delta\phi + \delta\ell|\}$. We restrict the time in this regime and consider the time evolution of the entanglement entropy after δt_0 .

At $\delta t \rightarrow \delta t_0$, $S_A^{(c)}$ is negatively divergent. From there it increases monotonically along with δt , and when δt becomes large (i.e., $\delta t \gg T_+^{-1}, |\delta\ell|, |\delta\phi|$),

$$S_A^{(c)} \simeq 2r_+ \delta t - r_- (2\delta\phi + \delta\ell) - 2 \log(\pi^2 T_+ T_-) + 2 \log r_\infty^2. \quad (17)$$

Therefore in this setup, we always experience a transition from the connected phase to the disconnected one.

C. $(1_{++}, 1_{--})$

As we noted in section III, the boundary of 1_{--} is completely timelike to that of 1_{++} , and so it is not reasonable to consider the entanglement between 1_{++} and 1_{--} .

V. DISCUSSIONS

In this short letter, we discussed the entanglement in the pairs of $(1_{++}, 1_{+-})$ or $(1_{++}, 1_{--})$ boundaries, by

⁴ In [3], this limit is taken implicitly. This can be explicitly given as the scale transformation of AdS₃, as

$$\phi = \Lambda^{-1} \tilde{\phi}, \quad t = \Lambda^{-1} \tilde{t}, \quad r = \Lambda \tilde{r}, \quad (15)$$

where $\Lambda \rightarrow \infty$. Then in terms of $\tilde{\phi}$, the periodicity is $2\pi\Lambda \rightarrow \infty$. Accordingly, the parameters of our black hole and subsystem A are also written as

$$\begin{aligned} r_\pm &= \Lambda \tilde{r}_\pm, \quad T_\pm = \Lambda \tilde{T}_\pm, \quad r_\infty = \Lambda \tilde{r}_\infty, \\ \phi_i &= \Lambda^{-1} \tilde{\phi}_i, \quad t_i = \Lambda^{-1} \tilde{t}_i, \quad \ell_i = \Lambda^{-1} \tilde{\ell}_i, \end{aligned} \quad (16)$$

and we regard the tilded quantities as $\mathcal{O}(\Lambda^0)$. This means a huge black hole in the bulk and tiny intervals on the boundary. We omit tildes hereafter.

³ The authors thank J. Maldacena for explaining this point.

computing the entanglement entropy of the union of two intervals A_1 and A_2 . In $(1_{++}, 1_{+-})$ case, we have two candidates for the minimal surfaces — connected and disconnected ones —, and we can also have a freedom of the winding n around the periodicity (A9), for the connected surface. Phase transition between the two phases may or may not happen, depending on the parameters $T_{\pm}, \delta\phi$ and $\delta\ell$. In particular, in the near-extremal regime ($T_+ \rightarrow 0$), the disconnected phase is always favored and no transition takes place. In $(1_{++}, 1_{--})$ case, the story is complicated because of the counterintuitive winding modes which contribute negatively to the spacelike distance. After removing them by decompactification, we find that the phase transition always occurs.

We can also write down the entanglement entropies for $(1_{++}, 3_{\eta_1\eta_2})$ pairs. However, the periodicity (A9) makes problems again, because it is clearly a closed timelike curve and so it is doubtful whether such sectors have physically consistent description as a field theory. Furthermore, since the boundaries of region 3 are surrounded by the conical singularities (see FIG. 2 (a)), we are not sure that we can rely on the standard prescription of the minimal area surface. The naive computation itself is an easy problem by using TABLE III, and we leave it to the reader.

In this letter, we analyzed the relation between entanglement and multi-boundary connected spacetime in the three dimensional bulk. It would be interesting to generalize this to higher dimensional spacetime. For deeper understanding of how generic multi-boundary spacetime are emerging related to the boundary entanglement like [4], we need to find a proper interpretation or counterparts of these results in the boundary CFT. Hopefully, we would return to these problems in near future.

Acknowledgments

This work was supported by RIKEN iTHES Project. NI is also supported in part by JSPS KAKENHI Grant Number 25800143. NO thanks RIKEN Mathematical Physics Laboratory for hospitality while this work was being completed. NO is also grateful to Kimyeong Lee, Futoshi Yagi, Zhaolong Wang, Sang-Jin Sin, Jae-Hyuk Oh, Shigenori Seki, Yunseok Seo and Yang Zhou for comments and discussions.

Appendix A: Spacetime Structure of Maximally Extended Rotating BTZ

In this appendix, we briefly review the spacetime structure of the rotating BTZ black hole. Large part of the contents here was examined in [7], and we use basically the same notation as theirs.

The AdS_3 spacetime is given as an $\mathbb{R}^{2,2}$ -embedded hy-

perboloid, expressed by

$$\begin{aligned} x_0^2 + x_1^2 - x_2^2 - x_3^2 &= R^2, \\ ds^2 &= -dx_0^2 - dx_1^2 + dx_2^2 + dx_3^2. \end{aligned} \quad (\text{A1})$$

It is obvious that this space is invariant under $\text{SO}(2, 2) \simeq \text{SL}(2, \mathbb{R}) \times \text{SL}(2, \mathbb{R})$, and the AdS boundary is given by

$$x_0^2 + x_1^2 \rightarrow \infty, \quad x_2^2 + x_3^2 \rightarrow \infty. \quad (\text{A2})$$

We take the AdS radius $R = 1$ hereafter. By introducing U and V as

$$U = x_1^2 - x_2^2, \quad V = x_0^2 - x_3^2, \quad (\text{A3})$$

the AdS hyperboloid (A1) represents a straight line on the (U, V) -plane,

$$U + V = 1. \quad (\text{A4})$$

At the same time, (A3) can be regarded as hyperbolae on (x_1, x_2) - and (x_0, x_3) -planes for each fixed pair (U, V) . That is, each point (U, V) on the line (A4) represents the direct product of a pair of these hyperbolae. At $(U, V) = (1, 0)$ and $(0, 1)$, one of these two hyperbolae becomes a pair of straight lines crossing at the origin. Note that from (A4), we can decompose (U, V) -plane into three regions, 1: $U \geq 0, V \leq 0$, 2: $U \geq 0, V \geq 0$, and 3: $U \leq 0, V \geq 0$. This decomposition will be used later.

In this context of (A3), the AdS boundary (A2) corresponds to going to infinity on either (or both) of (x_1, x_2) - and (x_0, x_3) -planes along with the hyperbolae. Therefore obviously, every point (U, V) on (A4) touches the AdS boundary.

The BTZ black hole (1) is obtained as an orbifold,

$$\begin{aligned} \begin{pmatrix} x_1 \\ x_2 \\ x_3 \\ x_0 \end{pmatrix} &\simeq \begin{pmatrix} \cosh \gamma_+ & \sinh \gamma_+ & 0 & 0 \\ \sinh \gamma_+ & \cosh \gamma_+ & 0 & 0 \\ 0 & 0 & \cosh \gamma_- & \sinh \gamma_- \\ 0 & 0 & \sinh \gamma_- & \cosh \gamma_- \end{pmatrix} \begin{pmatrix} x_1 \\ x_2 \\ x_3 \\ x_0 \end{pmatrix}, \\ \gamma_{\pm} &= \pm 2\pi r_{\pm}, \end{aligned} \quad (\text{A5})$$

of the global AdS_3 spacetime (A1). This orbifolded spacetime can be covered by using 12 patches, each of which has the metric of the form of (1). Those are:

Region 1: (outside the black hole, $r \geq r_+$.)

$$x_1 = \eta_1 \left(\frac{r^2 - r_-^2}{r_+^2 - r_-^2} \right)^{1/2} \cosh(\pi (T_+ u^+ + T_- u^-)), \quad (\text{A6a})$$

$$x_2 = \eta_1 \left(\frac{r^2 - r_-^2}{r_+^2 - r_-^2} \right)^{1/2} \sinh(\pi (T_+ u^+ + T_- u^-)), \quad (\text{A6b})$$

$$x_3 = \eta_2 \left(\frac{r^2 - r_+^2}{r_+^2 - r_-^2} \right)^{1/2} \cosh(\pi (T_+ u^+ - T_- u^-)), \quad (\text{A6c})$$

$$x_0 = \eta_2 \left(\frac{r^2 - r_+^2}{r_+^2 - r_-^2} \right)^{1/2} \sinh(\pi (T_+ u^+ - T_- u^-)), \quad (\text{A6d})$$

Hereafter $u^\pm = \phi \pm t$, and the pair (η_1, η_2) takes $(+, +)$, $(+, -)$, $(-, +)$, $(-, -)$. This region 1 covers all the sign of x_1 and x_3 in the (U, V) -plane with $U > 0, V \leq 0$.

Region 2: (between the outer and inner horizons, $r_- \leq r \leq r_+$.)

$$x_1 = \eta_1 \left(\frac{r^2 - r_-^2}{r_+^2 - r_-^2} \right)^{1/2} \cosh(\pi (T_+ u^+ + T_- u^-)), \quad (\text{A7a})$$

$$x_2 = \eta_1 \left(\frac{r^2 - r_-^2}{r_+^2 - r_-^2} \right)^{1/2} \sinh(\pi (T_+ u^+ + T_- u^-)), \quad (\text{A7b})$$

$$x_3 = \eta_2 \left(\frac{r_+^2 - r^2}{r_+^2 - r_-^2} \right)^{1/2} \sinh(\pi (T_+ u^+ - T_- u^-)), \quad (\text{A7c})$$

$$x_0 = \eta_2 \left(\frac{r_+^2 - r^2}{r_+^2 - r_-^2} \right)^{1/2} \cosh(\pi (T_+ u^+ - T_- u^-)), \quad (\text{A7d})$$

This region 2 covers $U \geq 0, V \geq 0$ in the (U, V) -plane. Note that from region 1 to region 2, the range of r changes from $r \geq r_+$ to $r \leq r_+$, and the sign of $V = x_0^2 - x_3^2$ changes, while the sign of $U = x_1^2 - x_2^2$ unchanged. This explains the r -dependent factor changes and the ‘‘sinh’’-‘‘cosh’’ flip between (A6c) and (A7c), and between (A6d) and (A7d).

Region 3: (inside the inner horizon, $r \geq r_+$.)

$$x_1 = \eta_1 \left(\frac{r^2 - r_+^2}{r_+^2 - r_-^2} \right)^{1/2} \sinh(\pi (T_+ u^+ - T_- u^-)), \quad (\text{A8a})$$

$$x_2 = \eta_1 \left(\frac{r^2 - r_+^2}{r_+^2 - r_-^2} \right)^{1/2} \cosh(\pi (T_+ u^+ - T_- u^-)), \quad (\text{A8b})$$

$$x_3 = \eta_2 \left(\frac{r^2 - r_+^2}{r_+^2 - r_-^2} \right)^{1/2} \sinh(\pi (T_+ u^+ + T_- u^-)), \quad (\text{A8c})$$

$$x_0 = \eta_2 \left(\frac{r^2 - r_+^2}{r_+^2 - r_-^2} \right)^{1/2} \cosh(\pi (T_+ u^+ + T_- u^-)). \quad (\text{A8d})$$

This region 3 covers $U \leq 0, V > 0$ in the (U, V) -plane. Note that region 1 and region 3 are related by $U (= x_1^2 - x_2^2)$ and $V (= x_0^2 - x_3^2)$ exchange, therefore, region 1's (x_1, x_2, x_3, x_0) and region 3's (x_0, x_3, x_2, x_1) are exchanged⁵.

Depending on these signs, we refer each of the 12 regions as $1_{++}, 2_{+-}$, etc. It can be easily shown that each of the embeddings (A6)(A7)(A8) leads to the same induced metric (1), while the orbifold (A5) becomes

$$\phi \simeq \phi + 2\pi \quad (\text{for region 1,2}), \quad (\text{A9a})$$

$$t \simeq t + 2\pi \quad (\text{for region 3}). \quad (\text{A9b})$$

⁵ This explains relations between (A6a) and (A8d), (A6b) and (A8c), (A6c) and (A8b), and (A6d) and (A8a).

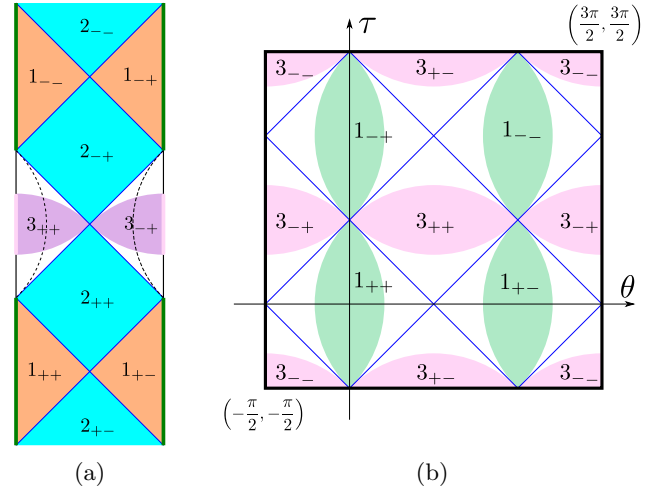


FIG. 2: (a) The Penrose diagram of the rotating BTZ black hole with a two-dimensional (t, r) plane set by $d\phi = N(r)dt$. Dashed lines represent BTZ (conical) singularity.

(b) The boundary in terms of global coordinate (θ, τ) , where θ, τ have 2π periodicity. BTZ identifications (A9) restricts the fundamental domains as the colored areas. The diagonal blue lines represent region 2.

(These two figures are essentially copies of Fig.4 and Fig.5 in [7], respectively.)

Due to the $t \simeq t + 2\pi$ identification in region 3, there is a conical singularity at the radius $r = \sqrt{r_+^2 + r_-^2}$, where $g_{tt} = 0$ in region 3. The Penrose diagram for this space-time can be drawn as FIG. 2 (a)⁶.

Since every point (U, V) reaches to the AdS boundary, the AdS boundary is also divided into the 12 different regions $1_{\eta_1\eta_2}, 2_{\eta_1\eta_2}$ and $3_{\eta_1\eta_2}$, although the region 2 becomes just straight-lines on the boundary. The arrangements of $1_{\eta_1\eta_2}$ and $3_{\eta_1\eta_2}$ on the AdS global coordinate boundary, can be seen, from $\tan\left(\frac{\theta \pm \tau}{2}\right)\Big|_{\mu \rightarrow \infty} = (\tanh(\pi T_\pm u_\pm))^{\eta_1\eta_2}\Big|_{r \rightarrow \infty}$ for region 1, and $\tan\left(\frac{\theta \pm \tau}{2}\right)\Big|_{\mu \rightarrow \infty} = (\pm \tanh(\pi T_\pm u_\pm))^{\mp \eta_1\eta_2}\Big|_{r \rightarrow \infty}$ for region 3. The fact that $|\tanh(\pi u_\pm T_\pm)| \leq 1$ gives the restriction for the allowed parameter range in the (θ, τ) plane, and determines whether each boundary point belongs to region $1_{\eta_1\eta_2}$, or region $3_{\eta_1\eta_2}$. The configurations of each region on the AdS boundary is drawn in FIG. 2 (b).

Appendix B: Analytic Continuations

The different patches (A6)(A7)(A8) can be connected to one another, by various analytic continuations of (t, ϕ, r) or (u^\pm, r) coordinates to complex-valued regions.

⁶ Note that this diagram represents the null surface but the trajectory of the light is not necessary on this diagram, due to the constraint $d\phi = N(r)dt$.

| | u^+ | u^- | r |
|----------|-------------------------|-------------------------|---------------------------------|
| 2_{++} | $u^+ - \frac{i}{4T_+}$ | $u^- + \frac{i}{4T_-}$ | r |
| 2_{--} | $u^+ + \frac{3i}{4T_+}$ | $u^- + \frac{i}{4T_-}$ | r |
| 2_{+-} | $u^+ + \frac{i}{4T_+}$ | $u^- - \frac{i}{4T_-}$ | r |
| 2_{-+} | $u^+ - \frac{3i}{4T_+}$ | $u^- - \frac{i}{4T_-}$ | r |
| 3_{++} | $u^+ - \frac{i}{2T_+}$ | $-u^-$ | $i\sqrt{r^2 - (r_+^2 + r_-^2)}$ |
| 3_{--} | $u^+ + \frac{i}{2T_+}$ | $-u^-$ | $i\sqrt{r^2 - (r_+^2 + r_-^2)}$ |
| 3_{+-} | u^+ | $-u^- - \frac{i}{2T_-}$ | $i\sqrt{r^2 - (r_+^2 + r_-^2)}$ |
| 3_{-+} | u^+ | $-u^- + \frac{i}{2T_-}$ | $i\sqrt{r^2 - (r_+^2 + r_-^2)}$ |

TABLE III: Analytic continuations from 1_{++} to $2_{\eta_1\eta_2}$ and $3_{\eta_1\eta_2}$, up to the periodicity $(u^+, u^-) \simeq (u^+ + i/T_+, u^- \pm i/T_-)$. In region 2, we promise that $(r^2 - r_+^2)^{1/2} = i(r_+^2 - r^2)^{1/2}$.

The list of the ones from 1_{++} to $1_{\eta_1\eta_2}$ is given in TABLE I. For completeness, we list the other formula of analytic continuations in TABLE III.

-
- [1] M. Van Raamsdonk, (2009), arXiv:0907.2939 [hep-th] .
- [2] M. Van Raamsdonk, Gen.Rel.Grav. **42**, 2323 (2010), arXiv:1005.3035 [hep-th] .
- [3] T. Hartman and J. Maldacena, JHEP **1305**, 014 (2013), arXiv:1303.1080 [hep-th] .
- [4] J. Maldacena and L. Susskind, (2013), arXiv:1306.0533 [hep-th] .
- [5] S. Ryu and T. Takayanagi, Phys.Rev.Lett. **96**, 181602 (2006), arXiv:hep-th/0603001 [hep-th] .
- [6] S. Ryu and T. Takayanagi, JHEP **0608**, 045 (2006), arXiv:hep-th/0605073 [hep-th] .
- [7] S. Hemming, E. Keski-Vakkuri, and P. Kraus, JHEP **0210**, 006 (2002), arXiv:hep-th/0208003 [hep-th] .
- [8] V. E. Hubeny, M. Rangamani, and T. Takayanagi, JHEP **07**, 062 (2007), arXiv:0705.0016 [hep-th] .
- [9] J. M. Maldacena, JHEP **0304**, 021 (2003), arXiv:hep-th/0106112 [hep-th] .
- [10] M. Headrick, Phys.Rev. **D82**, 126010 (2010), arXiv:1006.0047 [hep-th] .
- [11] T. Andrade, S. Fischetti, D. Marolf, S. F. Ross, and M. Rozali, (2013), arXiv:1312.2839 [hep-th] .